Molecular Therapy
Original Article

# Pre-arrayed Pan-AAV Peptide Display Libraries for Rapid Single-Round Screening

Kathleen Börner,[1,2,10] Eike Kienle,[1,7,10,11] Lin-Ya Huang,[3] Jonas Weinmann,[1,12] Anna Sacher,[4] Philipp Bayer,[1] Christian Stüllein,[5] Julia Fakhiri,[1] Laura Zimmermann,[4] Adrian Westhaus,[1] Jürgen Beneke,[6,7] Nina Beil,[6,7] Ellen Wiedtke,[1,7] Carolin Schmelas,[1] Dominik Miltner,[1] Alexander Rau,[1] Holger Erfle,[6,7] Hans-Georg Kräusslich,[1,2,7,8] Martin Müller,[4] Mavis Agbandje-McKenna,[3] and Dirk Grimm[1,2,7,9]

[1]Department of Infectious Diseases/Virology, BioQuant Center, Heidelberg University Hospital, Im Neuenheimer Feld 267, 69120 Heidelberg, Germany; [2]German Center for Infection Research (DZIF), Heidelberg, Germany; [3]Department of Biochemistry and Molecular Biology, Center for Structural Biology, McKnight Brain Institute, University of Florida, Gainesville, FL 32610, USA; [4]German Cancer Research Center (DKFZ), F035, Im Neuenheimer Feld 242, 69120 Heidelberg, Germany; [5]CLADIAC GmbH, Kurfürsten-Anlage 52-58, 69115 Heidelberg, Germany; [6]BioQuant Center, University of Heidelberg, Im Neuenheimer Feld 267, 69120 Heidelberg, Germany; [7]Cluster of Excellence CellNetworks, 69120 Heidelberg, Germany; [8]Department of Infectious Diseases/Virology, Center for Integrative Infectious Disease Research (CIID), Heidelberg University Hospital, Im Neuenheimer Feld 344, 69120 Heidelberg, Germany; [9]German Center for Cardiovascular Research (DZHK), Heidelberg, Germany

**Display of short peptides on the surface of adeno-associated viruses (AAVs) is a powerful technology for the generation of gene therapy vectors with altered cell specificities and/or transduction efficiencies. Following its extensive prior use in the best characterized AAV serotype 2 (AAV2), recent reports also indicate the potential of other AAV isolates as scaffolds for peptide display. In this study, we systematically explored the respective capacities of 13 different AAV capsid variants to tolerate 27 peptides inserted on the surface followed by production of reporter-encoding vectors. Single-round screening in pre-arrayed 96-well plates permitted rapid and simple identification of superior vectors in >90 cell types, including T cells and primary cells. Notably, vector performance depended not only on the combination of capsid, peptide, and cell type, but also on the position of the inserted peptide and the nature of flanking residues. For optimal data availability and accessibility, all results were assembled in a searchable online database offering multiple output styles. Finally, we established a reverse-transduction pipeline based on vector pre-spotting in 96- or 384-well plates that facilitates high-throughput library panning. Our comprehensive illustration of the vast potential of alternative AAV capsids for peptide display should accelerate their *in vivo* screening and application as unique gene therapy vectors.**

## INTRODUCTION

During the last 1.5 decades, adeno-associated virus (AAV) peptide display has become a powerful and versatile technology for the generation and selection of gene transfer vectors with tailored efficiency and/or cell specificity. It is based on the insertion of short, typically 7- to 9-aa-long peptides into a position on the viral capsid surface that alters natural cellular AAV interactions, with the aim to concurrently abrogate this property and retarget the engineered virus to a given cell or tissue type.[1,2] For this purpose, a preferred location for peptide insertion is the top of an AAV variable region (e.g., VR-VIII[3]) within the GH loop that protrudes from the external capsid surface and contributes to the formation of the 3-fold symmetry-related axis, which, in turn, is key to AAV-cell interactions. To bolster chances of success, this technique can be conducted in high throughput, starting with the creation of a comprehensive capsid library displaying millions of randomized peptides on the AAV surface (one sequence per capsid) from which desired candidates are then selected through iterative screening in target cells or tissues.[1,2,4,5]

The overall power of AAV peptide display has already been extensively validated *in vitro* and *in vivo*, using the best characterized serotype AAV2 as scaffold, with insertions after two of its exposed residues, i.e., asparagine at position 587 (N587) or the adjacent arginine 588 (R588). Together with four other amino acids, R588 is part of a capsid domain that mediates AAV2 binding to cellular heparan sulfate proteoglycans (HSPGs), explaining frequent observations that AAV2 variants with peptide modifications at these positions show differences in HSPG usage for transduction.[6] Typically, however, the receptors/interactions that are targeted by the peptide-engineered AAV2 variants remain enigmatic, as do the intracellular mechanisms underlying the altered viral properties. Notable exceptions were provided by the Büning laboratory, which had originally

Received 7 October 2019; accepted 8 February 2020;
https://doi.org/10.1016/j.ymthe.2020.02.009.

[10]These authors contributed equally to this work.

[11]Present address: University Medical Center, Johannes Gutenberg University Mainz, Hanns-Dieter-Huesch Weg 19, 55128 Mainz, Germany.

[12]Present address: Boehringer Ingelheim Pharma GmbH & Co. KG, Drug Discovery Sciences, J89.04.005, Birkendorfer Straße 65, 88400 Biberach an der Riß, Germany.

**Correspondence:** Dirk Grimm, Department of Infectious Diseases/Virology, BioQuant Center, Heidelberg University Hospital, BioQuant BQ0030, Im Neuenheimer Feld 267, 69120 Heidelberg, Germany.
**E-mail:** dirk.grimm@bioquant.uni-heidelberg.de

pioneered AAV peptide display along with the Trepel, Hallek, and Kleinschmidt laboratories,[7–9] and that identified αvβ8 integrin as receptor for a keratinocyte-specific AAV2,[10] as well as several laboratories that have recently reported an interaction of AAV-PHP.B (a peptide-modified AAV9) with the glycosylphosphatidylinositol (GPI)-linked protein LY6A.[11–13]

In spite of the recurrent successes with this technology in the AAV2 context, reports of its application in other AAV serotypes or capsid variants remain scarce. This includes display of pre-selected peptides, such as a biotin acceptor peptide in AAV1–AAV5,[14,15] a RGD motif in AAV1 or AAV6,[16,17] a $His_6$ tag in AAV8,[18] or cancer-targeting peptides in AAV8 or AAV9.[19] Concurrently, others created and selected non-AAV2 libraries displaying randomized peptides, including the Bennett and Kleinschmidt laboratories that used AAV8 as a scaffold to select in the murine retina[20] or liver.[21] Similarly, AAV9 was used by Varadi et al.[22] for screens in human coronary artery endothelial cells (HCAECs), or by Deverman et al.[23] for isolation of the aforementioned AAV-PHP.B, a capsid best known for its ability to cross the blood-brain barrier in C57BL/6 mice and to widely transduce neurons and astrocytes in the brain. Three additional studies have employed synthetic AAV variants for peptide display, namely, the chimera AAV-DJ[24,25] and a hybrid of AAV1 and AAV9 called AAV1.9-3.[26]

The scarcity of reports on peptide display outside of AAV2 is even more surprising in view of the mounting evidence, including data with AAV-DJ,[24] that the capsid that serves as a scaffold and the residues that flank the insertion can profoundly affect peptide and particle functionality. For instance, Ying et al.[27] identified peptides that improved AAV2 homing to murine heart tissue *in vivo* but noted their inability to likewise enhance AAV8 or AAV9. Similarly, Khabou et al.[28] transferred the 7m8 peptide, previously shown to boost AAV2 transduction of the retina in various animal models,[29] into AAV serotypes 5, 8, and 9, and they only observed a beneficial effect in the context of AAV9 but not the other two. As the final example, the Müller laboratory swapped peptides between AAV2 and AAV9 that were pre-selected in either context on HCAECs, and they found that such AAV cross-display typically strongly reduced transduction of the targeted cells.[22]

In this study, we comprehensively assessed the potential of 13 diverse AAV capsid variants, including AAV2 and 11 other viruses as well as the AAV-DJ chimera, for display of different pre-selected peptides and for particle retargeting in cultured cells. Our results demonstrate that alternative AAV capsids are versatile and powerful scaffolds for peptide display, and thereby inform and support their continued development as gene therapy vectors.

## RESULTS

### Engineering of 12 Different AAV Serotypes for Peptide Display

To study the capacity of various AAV serotypes as a scaffold for peptide display and vector production, we implemented and adhered to the following design rules. First, akin to the pioneering work in AAV2,[7–9] we chose to display peptides with a length of 7–9 aa because this range is well tolerated and sufficient for capsid retargeting. Second, we selected regions in all *cap* genes for in-frame oligonucleotide insertion that promised display of the encoded peptides in a prominent location, i.e., VR-VIII,[3] on the assembled particles. Third, to facilitate and expedite the preparation of all capsid genes for these insertions, we devised a cloning strategy that circumvents the successive, labor- and time-consuming mutagenesis steps that were originally implemented for AAV2.[8] The latter are illustrated in Figure 1A, which recapitulates the design reported in 2003 by the Kleinschmidt group[8] and later adapted by others, including us.[24] In this permutation, peptide-encoding oligonucleotides are inserted after the arginine at VP1 position 588 (R588) by harnessing two SfiI restriction sites that had been engineered into the AAV2 *cap*. SfiI was selected because it neither cleaves wild-type AAV2 nor the plasmid backbone, and it is a class IIP restriction enzyme whose cutting yields customizable sticky overhangs. This enables the deliberate production of two distinct ends that permit directional cloning of the oligonucleotide as two single-stranded DNAs that carry matching overhangs after annealing. SfiI is also a non-cutter in the 11 other serotypes modified in this study, i.e., AAV1, AAV3–AAV9, AAVrh.10, AAVpo.1, and AAV12, allowing us to apply the identical oligonucleotide insertion strategy in all of these variants.

As also seen in Figure 1A, introducing the two SfiI sites into AAV2 *cap* changed 1 aa upstream of the peptide insertion site, namely, N587 into Q (red in Figure 1A; also Table S1, AAV2 insertion site [i]). Hence, in the final modified AAV2 construct, the inserted peptide is flanked by GQR (left) and QAA (right), next to G (left) and A (right) that we used as spacers between the inserted peptide and the surrounding capsid sequence, to facilitate peptide display and folding (see also Figure 1C). To maximize comparability, we decided to maintain this design in all vectors that we aimed to derive from the 12 wild-type AAVs. However, while the N-to-Q mutation is the only change on the AAV2 amino acid level that results from inserting the two SfiI sites, more substantial alterations were needed in the 11 other serotypes (Table S1; Figure S1; Sequence S1). We thus devised a new approach (Figure 1B) in which a *cap* gene of interest is PCR amplified as two parts (each containing one SfiI site) that can be joined and inserted into an AAV2 *rep*-expressing helper plasmid via triple ligation, by using a central NsiI site (inherently absent in all 12 AAVs) and two unique flanking sites (SwaI upstream and SpeI downstream of the full-length *cap*; not shown in Figure 1B).

To validate the approach, we tested it with AAV2 *cap* using primers that amplified an ~1.8-kb left and an ~0.4-kb right part, based on a variant in which we had previously mutated R585 into a glutamine to reduce AAV2 binding to HSPG. Control digests and sequencing confirmed successful *cap* re-assembly and insertion of two SfiI sites in all tested clones (data not shown). Notably, the primers were designed to introduce a frameshift in the modified *cap* gene (Figures 1A and 1B, circled G), which is corrected upon insertion of a peptide-encoding oligonucleotide. This was based on our previous work where we had inserted randomized peptide libraries into AAV2 and wanted to reduce contamination of the viral library with

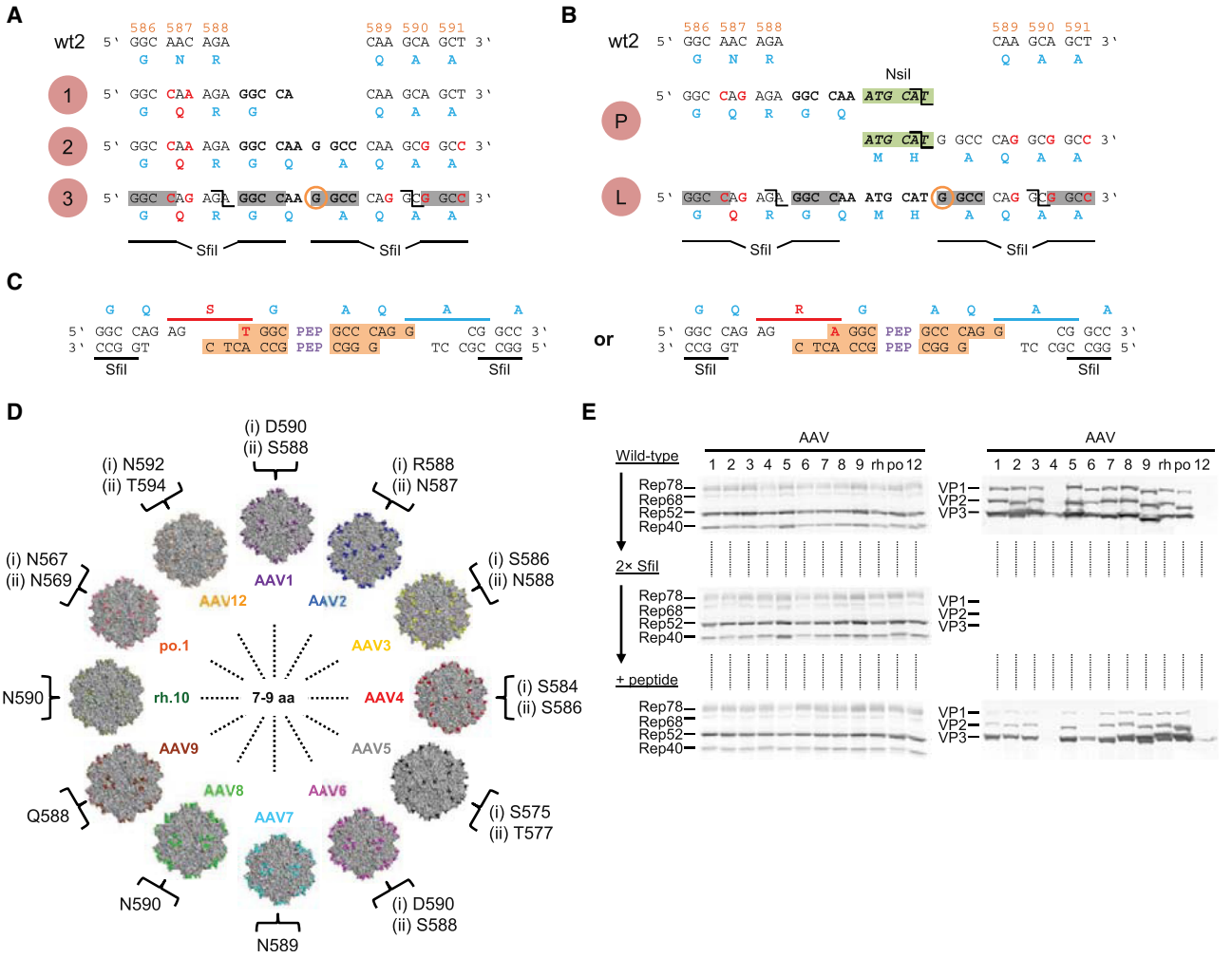


**Figure 1. Establishment of Peptide Display in 12 Different AAV Serotypes**

(A and B) Cloning strategy to introduce two SfiI sites into the different AAV *cap* genes (shown as an example is wild-type AAV2 [wt2]). For comparison, the conventional strategy requiring a series of site-directed mutagenesis steps is depicted in (A), versus the streamlined version established and used here (B). Numbers denote amino acid positions within VP1. Amino acids are shown in single-letter code. Nucleotides or amino acids that are changed at each step are highlighted in red. Also indicated are the SfiI binding and cleavage sites. The additional G nucleotide that causes a disrupting frameshift, which is corrected upon oligonucleotide insertion, is circled. In (B), P is the PCR step and L the ligation reaction. Highlighted in green are the NsiI sites that are used to join the two PCR products. (C) Two alternative designs of peptide-encoding oligonucleotides, resulting in either a serine (left) or arginine (right) upstream of the peptide (PEP). The overhangs highlighted in orange match those in the SfiI-restricted plasmid backbone. (D) Overview of all combinations of AAV serotypes and peptide insertion sites studied here (see also Table S1). (E) Confirmation of successful insertion or correction, respectively, of a frameshift in the *cap* gene of all 12 serotypes (see also A–C) by western blotting. Antibody 303.9 was used to detect all four Rep proteins in the left column and B1 for detection of VP1–VP3 in the right column. Note that VP1–VP3 expression is ablated in the clones containing the two SfiI restriction sites (2× SfiI) but no insert, and reconstituted upon insertion of peptide-encoding oligonucleotides (+ peptide). Also note that B1 does not detect VP1–VP3 of AAV4 or AAV12. Unmodified wild-type *cap* genes were used as positive controls at the top.

false positives, i.e., *cap* genes that had not taken up the oligonucleotide and thus did not display any peptide.[24] While not essential in the present context, we maintained this design to enable later use of all our newly engineered *cap* genes for random peptide display in a library format, too (see Discussion).

For verification, we inserted two annealed oligonucleotides encoding peptide NSSRDLG (D1 in Table S2; previously enriched from various AAV peptide display libraries[8,24]) into the SfiI sites of the modified AAV2 helper plasmid (Figure 1C). Upon ligation, the 5′ overhang changed R588 into a serine (left in Figure 1C, red) to further ablate HSPG binding. The success rate of ligation was 100%, and western blot analysis of small-scale vector productions validated restoration of VP1–VP3 protein expression after oligonucleotide insertion (data not shown). Taken together, this confirmed the feasibility, simplicity, and efficiency of our capsid modification strategy in the

AAV2 context, and it encouraged us to translate it into the other 11 serotypes.

To this end, we aligned their primary *cap* sequences to AAV2 and then harnessed our new PCR strategy (Figure 1B) to engineer peptide insertion sites within VR-VIII akin to R588 in AAV2 ([i] positions in Table S1, Figure 1D, and Figure S1; shown in detail in Sequence S1). As noted, the 11 primer pairs rendered the three residues flanking the insertion site on either side (third column in Table S1) identical to the engineered AAV2 *cap* (GQ[R or S, depending on the oligonucleotide]/QAA). This was expected to increase the probability that a given peptide would be displayed in a comparable manner at the tip of VR-VIII in all 12 serotypes. A small-scale production of all constructions with the D1-encoding peptide showed VP1–VP3 expression in the expected 1:1:10 ratio (Figure 1E). This validated the compatibility of the peptide insertion strategy with all AAV serotypes tested, and it motivated a subsequent expanded evaluation.

### Broader Analysis of Peptide-Capsid Combinations

First, we studied the display of a panel of six peptides (P1–P6, Table S2) originally isolated from phage or AAV2 display libraries and reported to retarget vectors to certain cell types in the AAV2 context (P1, PymT tumors;[30] P2, HeLa, K562, Raji, and SKOV-3 cells;[31] P3, MCF-7 and M07e cells;[9] P4/P5, human saphenous vascular endothelial cells [HSaVECs];[32] P6, MT1-MMP cells[33]). Of note, peptides P1–P3 share an RGD motif that is a consensus sequence for integrin binding, while P4 and P5 share a NDVR motif. P2 and P6 were selected by phage display and consist of 9 aa, instead of 7, as all other peptides including D1 that we used in our pilot studies. Therefore, these six peptides provided a variety of sequence lengths, motifs, and cell specificities. Here, we assessed whether and to what extent these peptides would alter target specificity of various non-AAV2 serotypes, and how, vice versa, capsid scaffolds other than AAV2 would affect peptide functionality.

By inserting P1–P6 into the 12 AAV serotypes, a total of 72 new AAV capsid-peptide variants were generated (Figure 2A). Together with the 12 parental sequences, they were used for small-scale packaging of a YFP (yellow fluorescent protein) reporter driven by a CMV (cytomegalovirus) promoter, permitting quick and easy measurement of functionality via cell transduction. Western blotting confirmed the presence of comparable VP1–VP3 amounts in all vector preparations independent of peptide sequence or length. The exception was the P6 construct with low levels of VP expression in the cell lysate, irrespective of the serotype (Figure 2B, right). The three capsid proteins were found, however, in western blots of whole-cell pellets after transfection of P6-encoding plasmids (Figure 2B, left), and they were also detected in iodixanol- or cesium chloride-purified vector stocks (data not shown). Taken together, this suggests that P6-containing particles can assemble but during production become trapped in an intracellular structure or compartment from which they are inefficiently released during the preparation of crude cell lysates. We still included P6-expressing clones in our further analyses, as it was possible that the viral titers in crude lysates were below the detection limit of western blotting, yet in a range that would permit transduction of certain cells.

We first tested the set of 84 vectors in HeLa cells, as they are known to be amenable to transduction with several AAV serotypes. As the simultaneous generation of 84 purified vector stocks was overly demanding, we used small-scale preparations that were made in parallel and then administered in equal volumes, to maximize comparability (Figure 2B). Transduction was accomplished in a 96-well format, and YFP expression was measured 72 h later by automated microscopy (Figure 2C). In addition, to obtain more quantitative values for transduction efficiencies (percentages of YFP-positive cells) and for mean expression intensities per cell, we analyzed a second plate by fluorescence-activated cell sorting (FACS). For direct comparison with the microscopy data, the FACS results are displayed as heatmaps in Figures 2D and 2E in which the values are color-coded, ranging from 0% (black) to 100% (white). Lastly, we independently confirmed the YFP data by repeating the AAV productions and transductions with a second vector encoding a luciferase reporter (Figure 2F).

Notably, numerous peptide-displaying vectors gave nearly 100% transduction, akin to wild-type AAV2 that is very potent in HeLa cells. Many of these efficient variants were based on serotypes that have never been used systematically for peptide display (AAV1, AAV7, AAVrh.10) and/or that are largely inert in cultured cells (AAV7–AAV9, AAVrh.10). Particularly effective peptides were P2, P4, and P5, which consistently enhanced these five AAV serotypes (1, 7–9, rh.10), while they had no effect or even a detrimental effect on the other seven wild-types, including AAV2. Hence, this pilot experiment revealed that (1) the activity of a displayed peptide critically depends on the AAV capsid, and that (2) non-AAV2 serotypes represent promising scaffolds for peptide display since they can be as efficient (or greater, see later examples) as the AAV2 prototype when decorated with certain peptides (in the used HeLa cells, P2, P4, and P5).

An additional interesting observation was that (3) the two parameters, transduction rate and expression level, did not automatically correlate, as exemplified with the pair of wild-types AAV2 and AAV6 (Figures 2C–2F). This is in line with the fact that AAV capsids differ in individual steps such as cell attachment, uptake, trafficking, intracellular processing, and/or uncoating. To concurrently visualize these two important parameters, we devised the bubble chart format shown in Figure 2G and also used in our online database SPIRIT (superior peptide insertions for improved targeting; see the next section). Here, the size of the inner circle corresponds to transduction rates (from small to large) and the color indicates increasing expression levels (from black to green).

### Comprehensive Screening of Peptide-Capsid Combinations

Next, we further expanded our collection of capsid mutants by incorporating an additional set of 20 peptides that we chose from the literature or had identified in our own prior library screens

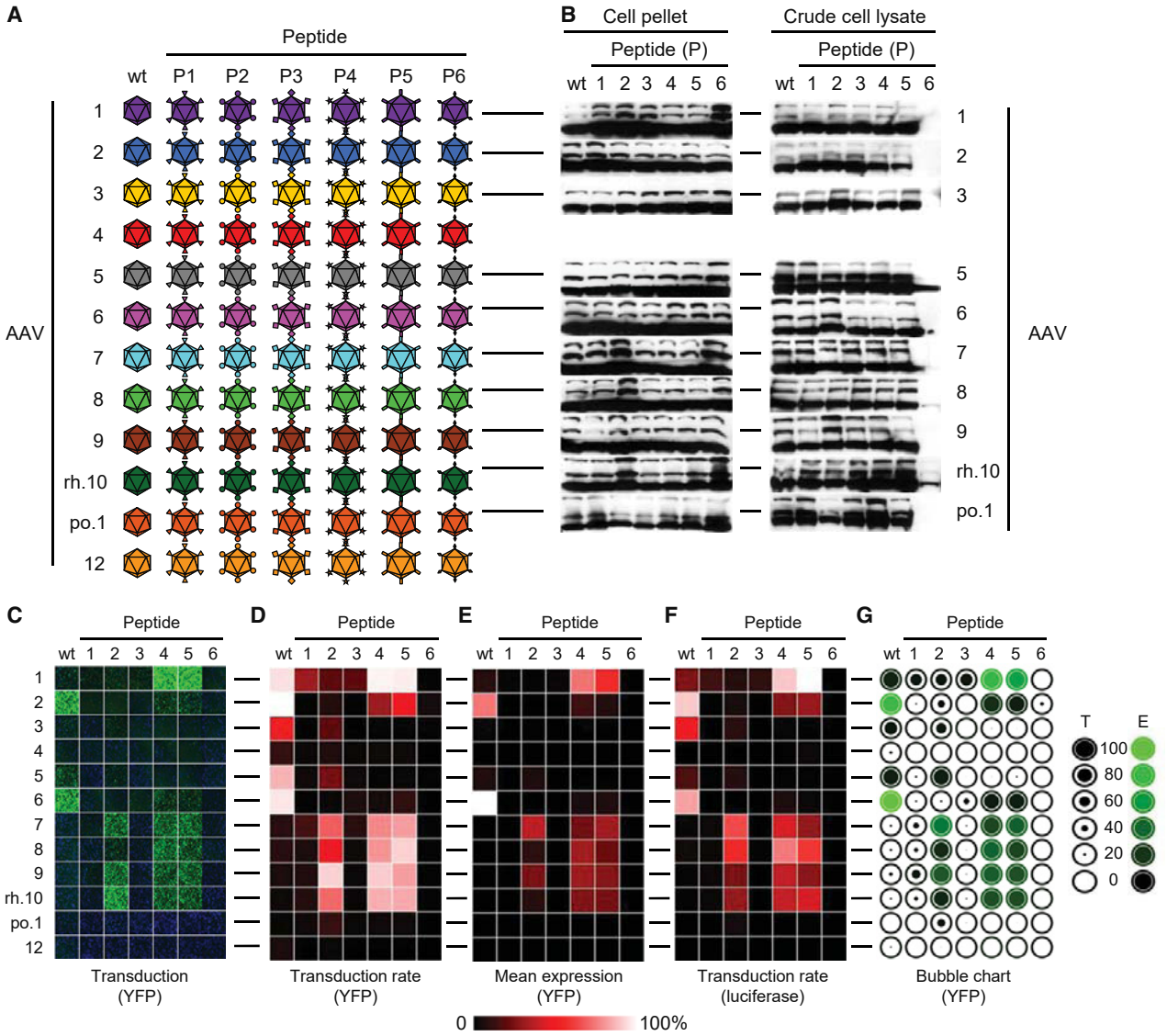


**Figure 2. Validation of the Feasibility to Express Peptides in 12 Different AAV Serotypes**

(A) Schematic overview of the panel of capsid-peptide combinations that was tested in this figure. See Table S2 for sequences of peptides P1–P6. (B) Confirmation of comparable VP expression and particle production. VP1–VP3 were detected using the B1 antibody in transfected cells (left) or cell supernatants after freeze-thaw cycles (right). Note that capsid proteins comprising peptide P6 were only detected in cell pellets but not in supernatants. (C–G) Functional validation through transduction of HeLa cells in 96-well format. Results are depicted as microscopic images of YFP expression (C), as heatmaps representing percentages of YFP-positive cells (D, transduction rate) or mean YFP expression measured via FACS (E), as a heatmap representing firefly luciferase expression (F), or as a bubble chart where the size of the inner circles represents the transduction rate and the intensity of the green color indicates the mean YFP expression (G). E, expression level; T, transduction rate.

(Table S2).[21,22,24,27,34,35] In addition, we structurally modeled a selection of peptides based on their energetically favored states in two representative AAV serotypes, AAV1 or AAV2, which suggested divergent peptide folding depending on sequence and scaffold (Figure 3) and hence distinct functionality. Interestingly, detailed modeling of VR-VIII showed that the insertion sites that we had originally chosen based on primary *cap* sequences (site [i] in Table S1; Figure S1) were shifted between the 12 serotypes. Specifically, we could distinguish the three groups shown in Figure 4 in which the insertion site was shifted by 1 or 2 aa to the left or the right, relative to the top of VR-VIII. As our pilot data (Figures 2C–2G) as well as follow-up experiments (see below and data in SPIRIT) consistently showed, the greatest peptide-mediated boost of transduction for serotypes 7–9 and rh.10, and as the insertion site in these four serotypes was in the identical position (group 2 in Figure 4), we adapted the other eight serotypes accordingly. To this end, we harnessed our

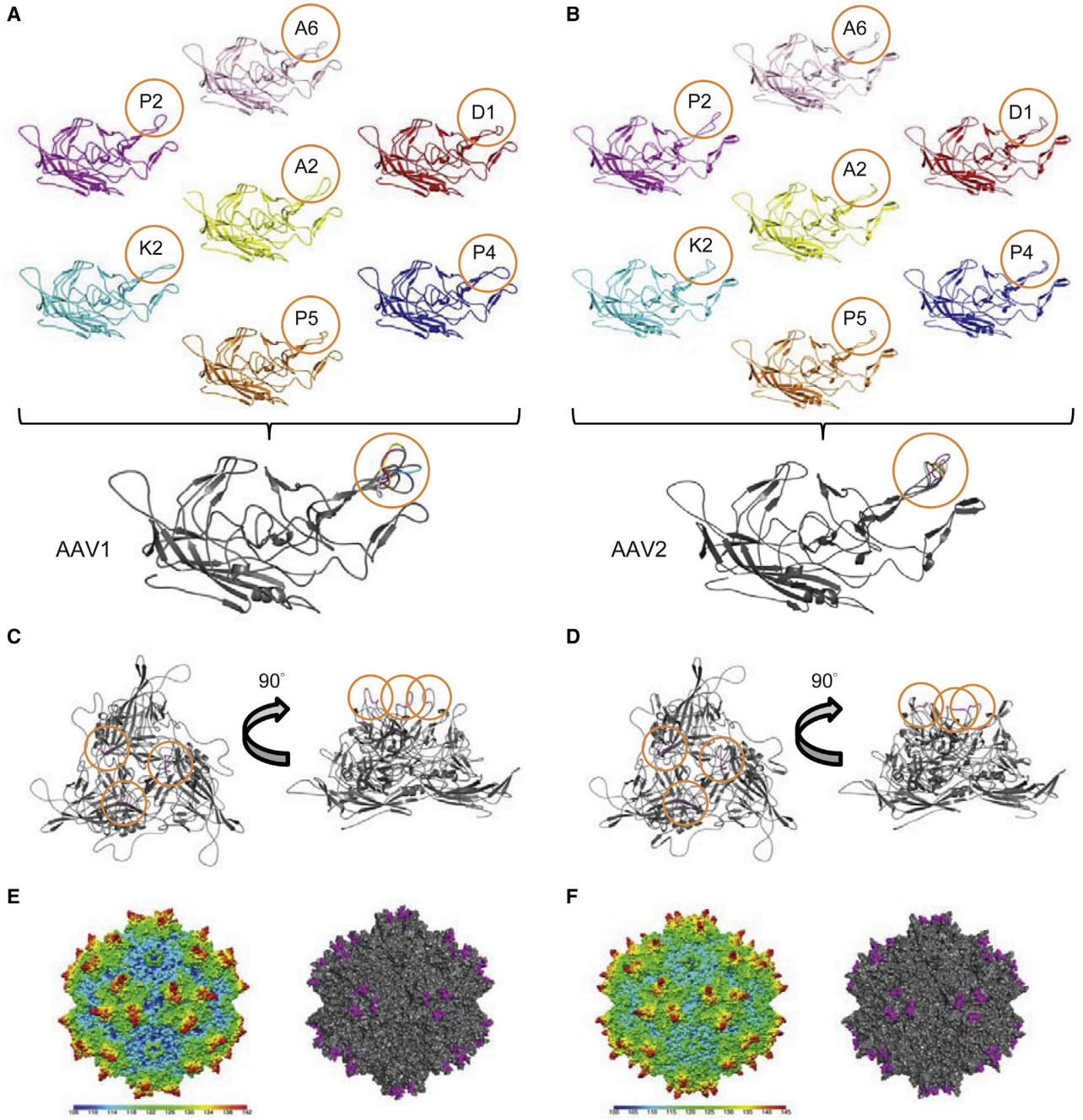


**Figure 3. Modeling of Selected Peptide Insertions in AAV1 or AAV2**

(A and B) Peptide-modified VP3 monomers of AAV1 (A) or AAV2 (B) comprising the seven peptides shown. Shown underneath are superimposed VP3 models. (C and D) Two views of a trimer of AAV1 (C) or AAV2 (D) VP3 containing peptide P2. Left: side view. Right: view down the three-fold symmetry axis. (E and F) Depth cue surface representation of the wild-type AAV1 (E) or AAV2 (F) capsid (left in each panel) or the derivative structure comprising the P2 peptide (right in each panel; P2 is shown in magenta). The color keys show the depth cue in Å. (A)–(D) and the right structures in (E) and (F) were generated in PyMOL.[36] The wild-type capsid structures shown on the left in panels (E) and (F) were generated in Chimera.[37]

PCR-based cloning strategy to shift the insertions in AAV1–AAV6, AAVpo.1, and AAV12 by 1 or 2 aa (site [ii] in Table S1; Figures S1 and 4; Sequence S1).

On top, we added our previously reported chimeric capsid AAV-DJ,[24] a hybrid of AAV serotypes 2, 8, and 9, as yet another scaffold for peptide display. Moreover, we extended the list of cells to more than 90

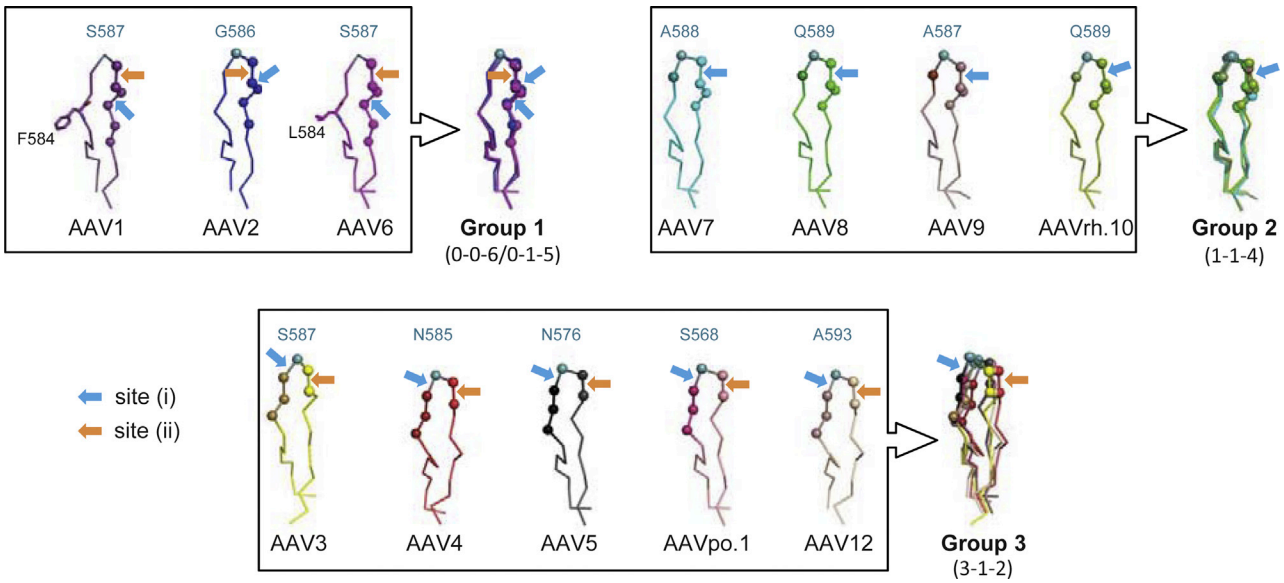


**Figure 4. Modeling of Peptide Insertion Sites in 12 Different AAV Serotypes**

Shown are the VR-VIII and the sites of peptide insertions. The latter are indicated by arrows, with site (i) shown in blue and site (ii) in orange. The six balls represent the amino acids flanking the insertion site (site [i], in case two were tested). The most protruded residue in each loop is colored in turquoise, and the corresponding residue is shown above. Values in brackets indicate the numbers of amino acids left of, at, or right of the peak of each loop (e.g., 1-1-4 denotes one residue left of the peak, one at the peak, and four right of the peak). Based on these characteristics, the modified capsids carrying insertion site (i) were segregated into the shown three groups. Note that insertion site (i) is slightly shifted in groups 1 and 3 as compared to group 2, while insertion site (ii) matches the position in group 2.

different types, comprising transformed or primary cells of mouse, rat, or human origin. We purposely included many that were found difficult to transduce in the past with AAV wild-type vectors, such as peripheral blood mononuclear cells, primary mouse or human myeloma (B cell tumor) cells, or primary human macrophages or dendritic cells. As before, all peptide-capsid combinations were produced in small scale and then used in different subsets to transduce the various target cells in 96-well plates, followed by microscopic or FACS readout of YFP reporter expression. Importantly, analyses of cell/nuclei counts by FACS or microscopy (data not shown) ruled out concerns about cell mortality following AAV transduction that could have created false-positive results.

To make the results of this extensive screening available in a comprehensive manner, we devised the database SPIRIT that is freely accessible online (http://spirit.cladiac.com/aav.html). Its graphical user interface offers a wide variety of options, including the ability to rank capsids by transduction efficiency within a single cell type, or to compare a given capsid across multiple cell types. The results can then be displayed as bubble charts akin to that in Figure 2G that concurrently depict transduction efficiencies and expression levels, or as bar graphs or tables (examples are shown in Figure S2). Importantly, SPIRIT is fully searchable, allowing users to either find a given capsid and then extract information on its activity across all cell types that it has been tested in to date, or, vice versa, to search for a favorite cell type and obtain a list or graphical representation of all capsids whose performance has already been assessed. In the future, we will continue to update SPIRIT with new AAV mutants and titration data as they become available in our laboratory.

As is evident from the data in SPIRIT as well as from the representative results shown in Figure S3, our major finding was that for all cell types tested, we could identify highly effective capsids. In most cases, the lead candidates were synthetic capsids that were modified by peptide insertion and that readily surpassed even the most potent wild types in these cells. Among the best examples are capsids AAV1P4, AAV1P5, AAV9A2, and AAVrh.10A2 that, for instance, were superior to all other AAV variants, including the 12 wild types in a collection of human T cell lines (Figure S3 and data in SPIRIT). A second notable candidate that we recognized through these screens is capsid AAV9P1 that performs exceptionally well in cultured human astrocytes[38] and also in various tissues in mice (J.W. and D.G., unpublished data). Finally, Figure 5 shows additional examples for robust transduction of primary cells or cell lines with AAV capsids that were identified in our screens, including a peptide display variant of AAV-DJ that excels in primary human macrophages (Figure 5C).

### Dissection of the Peptide Motif NXXRXXX

During our selection of peptides for display in the different serotypes, we noted that seven (P4, P5, A2, A6, D1, K2, L2; Table S2) shared the motif NXXRXXX (X, any amino acid). Interestingly, these peptides were consistently among the top transduction performers in the context of multiple serotypes and in numerous cell types (Figures 5

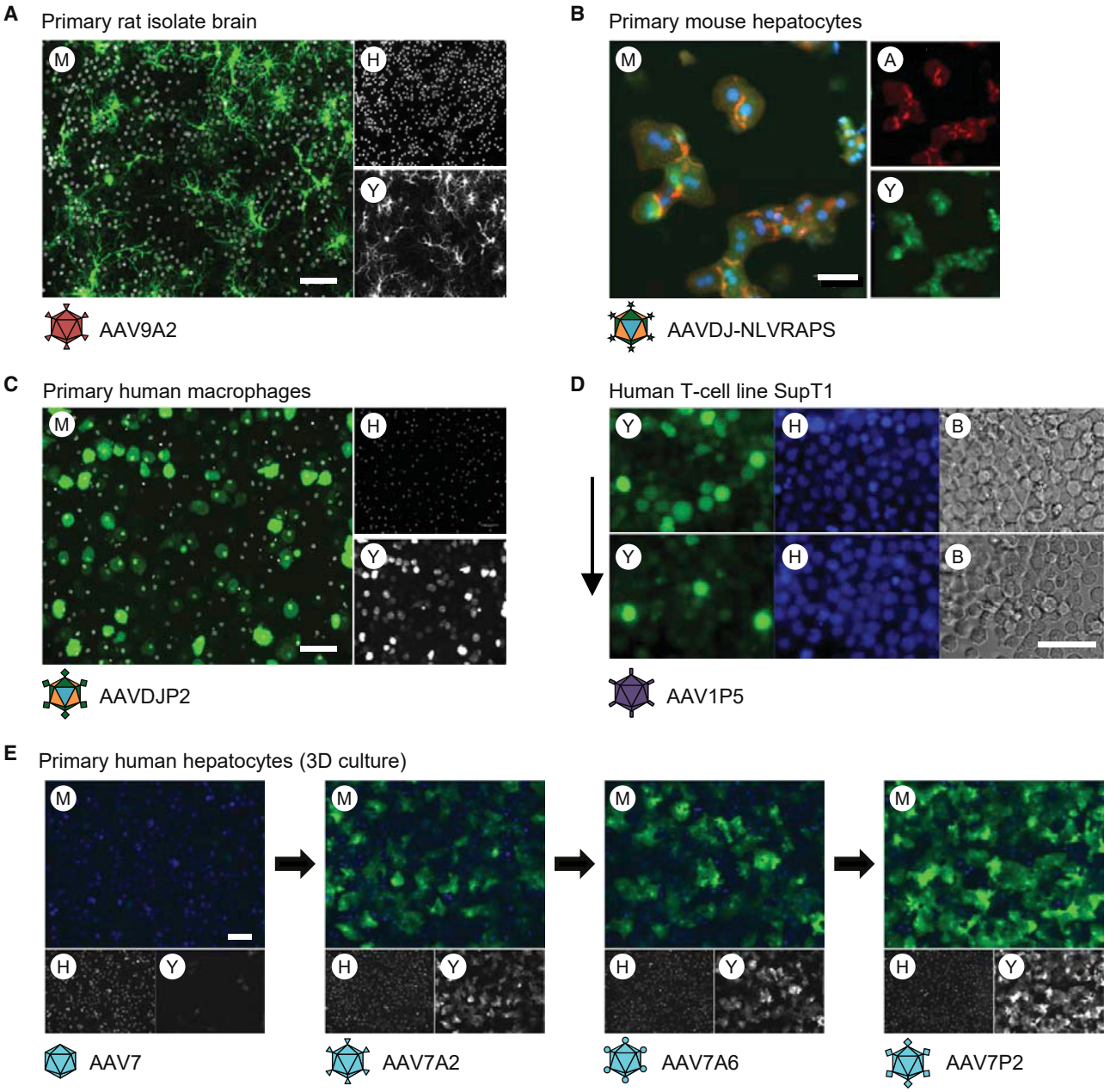


**Figure 5. Examples for Robust Transduction with Selected Capsid-Peptide Combinations**

Shown are representative fluorescence microscopy images of cells from different origins transduced with the indicated YFP-expressing AAV variant. Images were typically taken 2–3 days post-transduction. Letters in white circles denote (A) actin staining, (B) brightfield, (H) Hoechst staining of nuclei, (M) merge, or (Y) YFP expression. (A) Primary cortical neurons isolated from a rat on day 1 after birth. (B) Primary murine 3D hepatocyte culture transduced with one of the AAVDJ-NXXR peptide variants from Figure 6. The actin staining of canaliculi confirms the intact morphology of the hepatocytes. (C) Primary human monocyte-derived macrophages. (D) Human T cell line SupT1. The arrow indicates decreasing vector doses used for transduction (upper row, $1 \times 10^6$ vector genomes [vg]/cell; lower row, $1 \times 10^5$ vg/cell). (E) Primary human 3D hepatocytes transduced with wild-type AAV7 or its shown peptide-modified derivatives. Scale bars, (A), (C), and (E), 100 μm; (B) and (D), 50 μm.

and S3 and data in SPIRIT). Previously, others and we had noticed a frequent enrichment of NXXRXXX peptides in display libraries based on distinct serotypes, and we had also identified similar motifs in AAV-DJ, a very potent synthetic AAV capsid composed of multiple serotypes.[24] Here, we thus asked whether NXXRXXX peptides non-specifically enhance AAV transduction, and whether individual residues next to the N in position 1 and the R in position 4 are particularly critical.

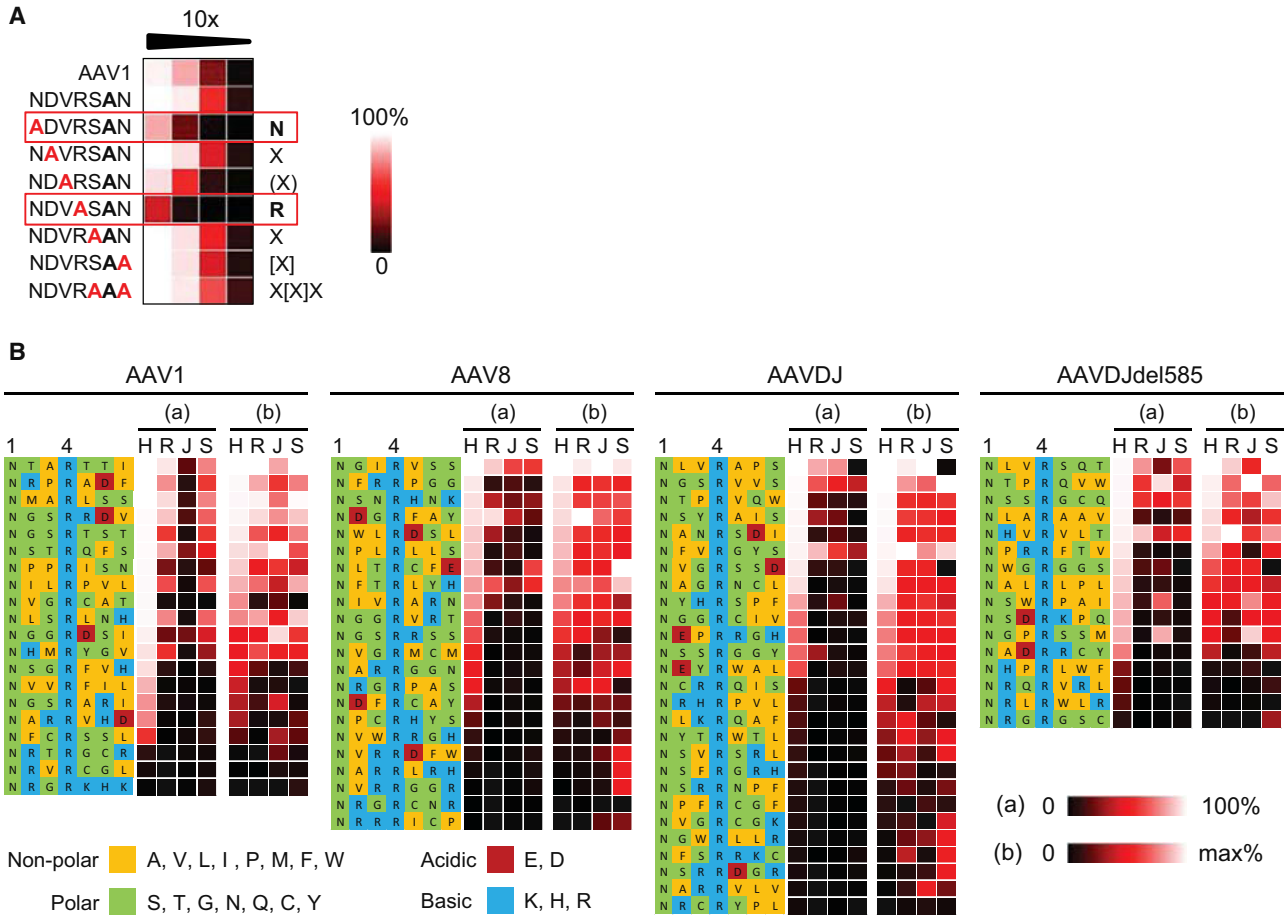


**Figure 6. Dissection of the Role of Individual Amino Acids in Peptides with an NXXRXXX Motif**

(A) Results of an alanine walk in peptide NDVRSAN (P4) in AAV1. Alanines that replace original residues are highlighted in red. All vectors were produced in parallel in small scale and used to transduce HeLa cells in a 96-well plate in 10-fold dilutions. Colors represent transduction rates. The two most critical residues whose change to alanine caused the largest drops in infectivity, N in position 1 and R in position 4, are boxed. The square brackets highlight the fact that in this peptide, residue 6 was alanine to begin with. (B) Results of screening of 85 vectors based on the shown four capsid scaffolds and displaying the indicated peptides in four cell types, i.e., HeLa (H), RAW (R), JAWS (J) and SupT1 (S). Transduction rates are depicted as heatmaps. In version (a), results in all four cell lines are shown at the same scale, whereas in (b), they are colored individually for each cell line, with white indicating the highest transduction rate that was measured within each line. Numbers 1 and 4 indicate residues N and R, respectively, that were kept constant in all peptides. The nature of individual residues is color-coded according to the legends at the bottom.

To resolve these possibilities, we first performed an alanine walk for peptide P4 (NDVRSAN) in AAV1 and measured transduction of the resulting seven mutants (including a double mutant of positions 5 and 7) in HeLa cells, in comparison to the original AAV1P4 and wild-type AAV1. Our finding that mutation of N or R in positions 1 or 4, respectively, impacted transduction by roughly 100-fold clearly highlights the relevance of these amino acids within the P4 peptide (Figure 6A). While a crucial role was also evident for V in position 3, albeit to a lesser extent, mutation of the remaining four positions (2, 5–7) had a negligible impact.

To perform these analyses in higher throughput, we generated several libraries based on AAV1, AAV8, and DJ expressing partially randomized NXXRXXX peptides in which only N and R remained constant. Therefore, we inserted the forward oligonucleotide AAC $(NNB)_2$ CGC $(NNB)_3$ where B can be nucleotides T, C, or G, while the residues N and R are encoded by AAC and CGC, respectively. Sanger sequencing of 211 arbitrarily selected bacterial colonies resulted in a set of 155 distinct NXXRXXX variants that are summarized in Table S3 (the remaining 56 clones either carried stop codons or gave ambiguous reads). Of these, we produced 85 as vectors and tested them in four different cell lines, i.e., HeLa, RAW, JAWS, and SupT1. The results depicted in Figure 6B illustrate four major findings. First, the comparison of each capsid variant across the four cell lines showed that highest transduction rates were usually obtained in HeLa cells, which was expected from their high susceptibility to AAV transduction. Second, and more interestingly, the most capsids were functional and effective, which became apparent when the color code of the heatmaps was individually adjusted for each cell line (right heatmaps in Figure 6B; the highest value within each

cell line is shown in white and the lowest in black). Third, the lead chimeras differed between the four cell lines, reaffirming that it is ultimately the combination of target cell, capsid, and peptide that governs transduction efficiency, congruent with and extending our other data. Finally, we noted that several peptides worked exclusively in a subset of the four tested cells types, exemplified by NVGRSSD whose display in AAV-DJ robustly enhanced transduction of HeLa cells and gave good results in Raji and Jurkat cells, but was inert in SupT1 cells. Similarly, display of NVGRCAT in AAV1 boosted transduction of HeLa cells but had no effect in the other three cell types. Taken together, this supports our conclusion that peptide display in AAV serotypes can concurrently alter efficiency and specificity of gene transfer.

### Role of the Number and Nature of Flanking Amino Acids

Up to this point, all AAV2 or AAV-DJ variants tested carried a glutamine at position 585 in combination with either a serine or arginine at position 588 (Q/S or Q/R). While the R585Q mutation had been introduced to reduce binding to the natural HSPG receptor, R588 that is also involved in HSPG attachment was changed into a serine in some of the peptide-modified capsids owing to insertion of a forward oligonucleotide starting with a T (Figure 1C). In all others, R588 was maintained due to an A at the start of the oligonucleotide that reconstituted the R-encoding AGA. To study whether and how these different mutations affect tropism, we cloned an additional set of 32 peptide-capsid combinations based on AAV2 or AAV-DJ in which we kept R585 and juxtaposed it with either R588 or S588 (Figure 7A). To this end, we selected eight peptides that we had already inserted into these two capsids (P2, P4, P5, A6, D1, T1, T2, K2) and now cloned the complementing forward oligonucleotide starting with T instead of A, or vice versa. We then produced and tested vectors based on the resulting 64 capsids (two serotypes × eight peptides × four residue pairs [Q/S, Q/R, R/S, R/R]) in 10 cell types.

The examples in Figures 7B and 7C illustrate a series of interesting observations. Most striking is that in the context of AAV2 but not AAV-DJ, R585 was frequently detrimental, as noted for five of the eight peptides (Figure 7C; A6, D1, T1, T2, K2). A curious exception is peptide P5 that was efficient in combination with R/S (next to Q/R and Q/S), but not R/R. In contrast, R/R gave the best results in most cells in the AAV-DJ context when juxtaposed with six of the eight peptides. Finally, P2 mostly worked best in juxtaposition with Q/R in AAV-DJ, and worst with R/R.

In this context, we became intrigued by a design reported in 2014 by Büning and colleagues[10] in which a 7-mer peptide—selected in human keratinocytes—was inserted after N587 (site [ii] here) in AAV2. In contrast to our own design, this peptide (Kera2, Table S2) was flanked by multiple alanines, i.e., three upstream and two downstream (Figure 7D, top), and the wild-type AAV2 amino acids were conserved on either side. To directly compare this design with our own, we inserted the same peptide into all 12 natural serotypes including AAV2 (insertion site [ii]) and then measured the activity of ensuing vector preparations in human keratinocytes (Figure 7D, bottom). Interestingly, within AAV2, we found that this peptide performed best in the reported AAA/AA context. Still, several other capsids from our collection surpassed the published variant, including the combination of this peptide with AAV1, AAV7, or AAVrh.10, as well as wild-type AAV6, which gave nearly 100% transduction (Figure 7D, bottom).

To further assess the impact of multiple flanking alanines, we recloned three of our peptides (A2, P2, P5) in the manner described above into AAV2 (illustrated for A2 in Figure 7E). Furthermore, we expanded the two downstream alanines to three or four. This extended the overall size of inserted foreign residues to up to 16, in the case of the 9-mer P2 with seven flanking alanines (three upstream and four downstream) (Table S4). Congruent with and expanding our prior data (Figures 7A–7C), analysis of all resulting vectors in six different cell types showed a strong dependency of the peptide on flanking amino acids. This is exemplified by the results in HeLa cells (Figure 7F), where A2 performed best in our own design in position 587 (Table S1, site [ii]), while the three combinations of flanking alanines reduced vector activity below that of wild-type AAV2. Yet, the results were strikingly different for P2, which worked best when embedded by three alanines on either side (i.e., a total of 15 foreign residues) (Figure 7F). Finally, P5 exhibited an equal preference for two or three downstream alanines (Figure 7F). Notably, we observed very similar tendencies in the other five tested cell lines (HEK293T, SF539, Huh7, MCF7, Vero; data not shown), implying that the variations in number and nature of flanking amino acids had exerted a peptide-specific, but cell type-unspecific, effect on vector functionality.

### Capsid Spotting and Screening by Reverse Transduction

The screens conducted above were performed in a liquid format, in which cells were plated first and then transduced with aliquots of vector suspension. While convenient for in-house screenings, we ultimately aimed to make our AAV panel available to the entire community, ideally in an easy-to-handle format that avoids shipping on dry ice and the associated freezing and thawing cycles. In particular, we envisioned the ability to spot the vectors onto 96- or 384-well cell culture plates, which could be shipped at room temperature and used for reverse transduction of cells that are plated on top of the dried vectors. We therefore tested a variety of conditions for spotting and for subsequent storage of the plates, using HeLa cells and microscopy or FACS analyses of YFP expression as readouts (Figure 8A). This led to a protocol that uses gelatin and fibronectin as a scaffold (see Materials and Methods for details), and that allows for extended storage of the spotted vectors (at least 1 month) at room temperature or −20°C without loss of functionality. Importantly, direct comparisons of transduction rates and mean YFP intensities between dried vectors or vectors in solution revealed a high correlation (Figures 8B–8D). Data were also largely comparable between vectors that were spotted onto 96- or 384-well plates (Figure 8D, middle versus right panel).

## DISCUSSION

A major reason for the popularity and success of AAV vectors is the availability of a wealth of technologies for engineering and

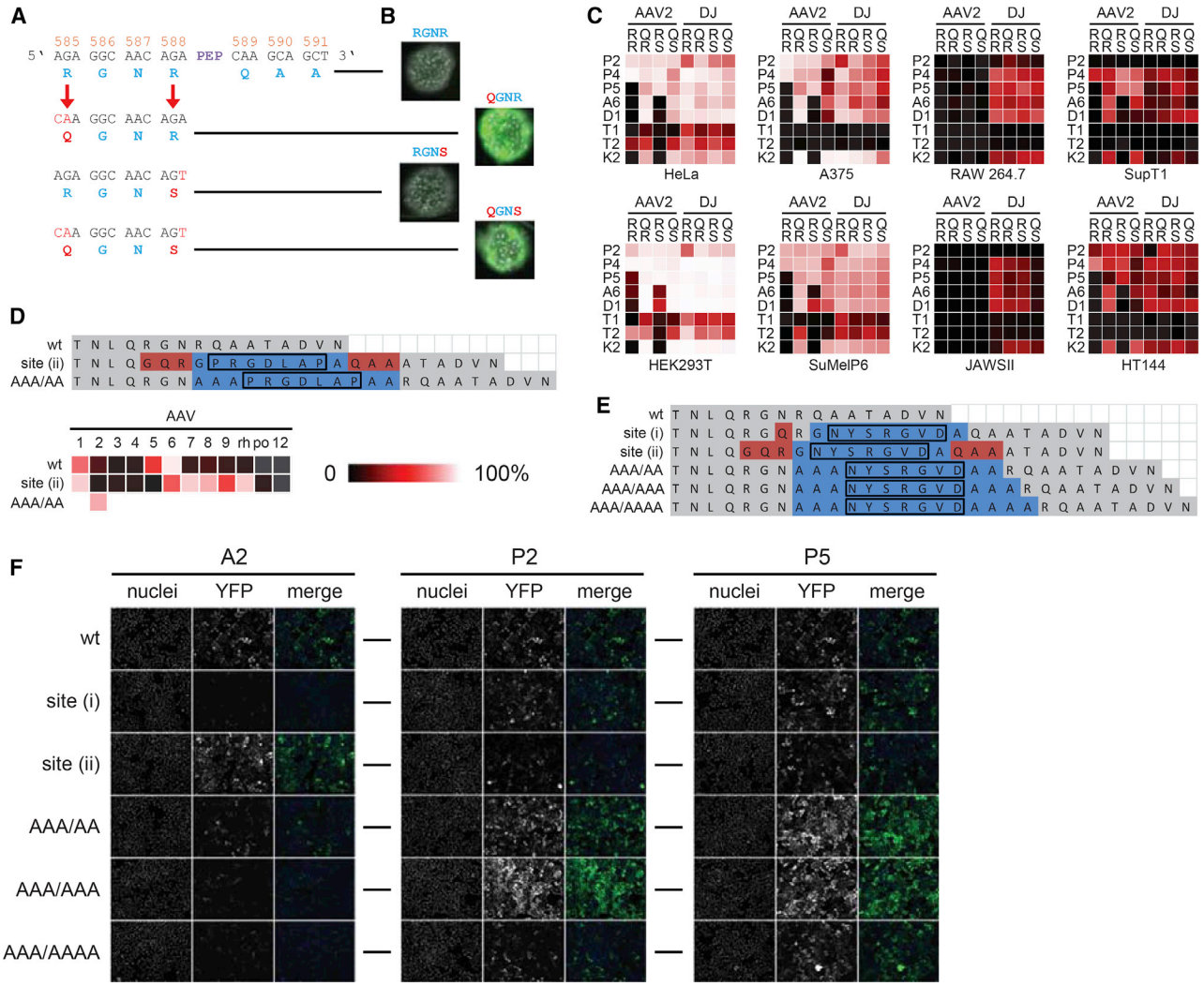


**Figure 7. Analysis of the role of residues in the AAV backbone flanking the peptide insertions**

(A and B) Effect of the arginines at position 585 or 588 in AAV2 or of their replacement with glutamine (R585Q) or serine (R588S), respectively, on transduction of cells (A; human liver organoids are shown as example in B). The inserted peptide in this example was K2. (C) Analysis of 64 peptide-capsid combinations based on AAV2 or AAV-DJ in which R585 or Q585 was juxtaposed with R588 or S588 in all possible permutations, and then combined with the shown eight peptides. The heatmaps illustrate transduction efficiencies measured in the indicated cell lines. (D) Comparison of insertion of a published keratinocyte-specific peptide (boxed) in AAV2 using our own strategy (site [ii]) or the reported design with multiple flanking alanines (AAA/AA). The heatmap shows the results of transduction of human keratinocytes. For comparison, the same peptide was inserted in 11 other serotypes as well, always using site (ii) when two were available. (E) Comparison of various combinations of amino acids flanking peptide insertions in AAV2. Shown in this example is peptide A2 (boxed). (F) Effect of the juxtaposition of the shown three peptides with the indicated flanking residues in AAV2 on transduction of HeLa cells.

repurposing the viral capsid.[1,2,4,5] Among these, the one that is in the center of the present study—peptide display—may be most attractive owing to its simplicity that enables its use in any laboratory equipped to perform standard molecular cloning. This distinguishes peptide display from alternative AAV evolution methodologies that are also powerful and versatile, but that are more time- and work-consuming, such as DNA family shuffling,[39] or that require specific bioinformatics expertise, such as ancestral reconstruction.[40,41] In view of this, it is surprising that only roughly a dozen studies to date[1] have applied peptide display in AAV serotypes other than the AAV2 prototype, in which it was originally established more than 15 years ago.[7–9]

Hence, the aim of our work was to close this gap by comprehensively evaluating peptide display technology in a total of 13 AAV variants, including 4 that we think have never been used for this purpose before, i.e., AAV7, AAVrh.10, AAVpo.1, and AAV12. Moreover, among the other nine, only a single peptide has reportedly ever been displayed in AAV3 and AAV4[15] as well as AAV6,[16] two in AAV5,[15,28] and three in

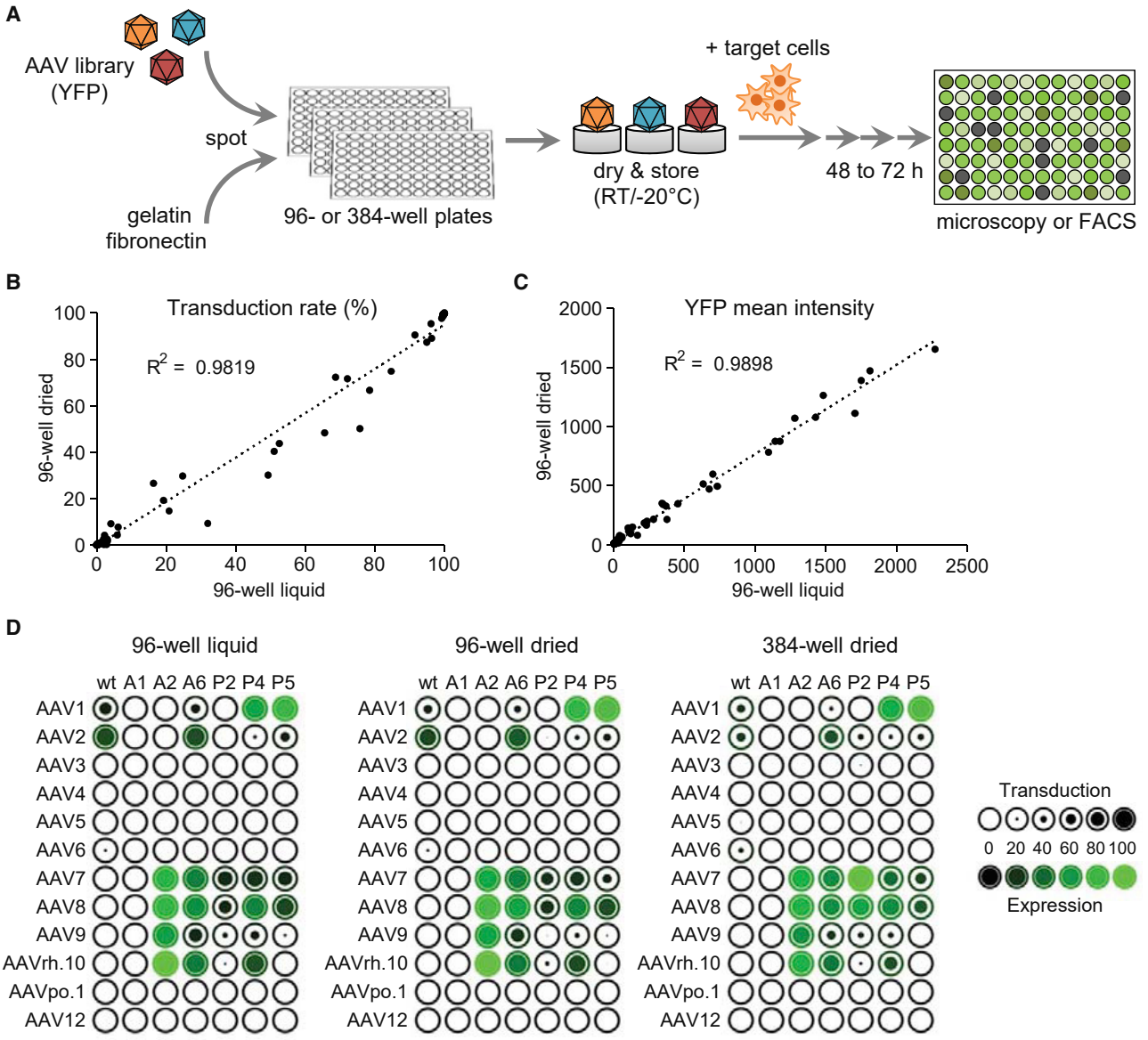


**Figure 8. Reverse Spotting/Transduction for Rapid and Simple AAV Capsid Screening**

(A) Workflow for AAV spotting and drying in 96- or 384-well plates, permitting long-term storage and shipping. (B and C) Correlation plots showing the transduction rates (B) and the mean YFP signals (C) of liquid versus reverse transduction in HeLaP4 cells in a 96-well format. Values per AAV mutant were averaged. Shown are linear regression analyses and R2 values, indicating the reproducibility between the two conditions. (D) Bubble charts corresponding to the data in (B) and (C) and depicting transduction rates and YFP expression levels. wt, wild-type.

AAV1.[15,17,42] Here, we juxtaposed 27 pre-selected peptides with the 13 AAV variants (not all possible combinations were tested) and furthermore displayed 85 partly randomized NXXRXXX peptides in four AAV capsids. Moreover, in 8 of the 13 AAV variants, we assessed two alternative peptide insertion sites and we also modified the flanking residues including HSPG-binding arginines in AAV2 and AAV-DJ. To this end, we particularly benefited from sequence and 3D structure predictions that we consider as accurate and highly reliable. We note that the conformation of the inserted peptides represents the energetically favored states of the peptides, which is the best possible approximation until we have an actual structure and thus know their true state. Altogether, this yielded more than 250 new capsid-peptide permutations. Subsequent measurement of the transduction efficiencies of various subsets of this collection in more than 90 cell types of various tissue and species origin (again, not all combinations were studied) resulted in a unique and rich dataset that we have made available online to the community, and that allows us to draw a series of important and encouraging conclusions.

First and foremost, our results illustrate the enormous potential of AAV serotypes other than AAV2 to serve as scaffolds for peptide display, evidenced by our finding that the ensuing vector variants often outperformed all wild types and AAV2 derivatives. Recently, this has already enabled our group and collaborators to conduct and publish a series of studies that critically benefitted from our original AAV-peptide combinations, and/or that would have been impossible without them. One example is work by Kunze et al.[38] who harnessed the juxtaposition of AAV9 with the P1 peptide to robustly and specifically deliver CRISPR machinery against latently integrated human immunodeficiency virus (HIV) genomes in cultured astrocytes, i.e., a major HIV reservoir in the brain. Similarly, Cordas Dos Santos et al.[43] exploited display of the A2 peptide in AAV9 and AAVrh.10 for efficient short hairpin (shRNA) expression in different T cell acute lymphoblastic leukemia cell lines. In two further examples, together with the Mhlanga or Kräusslich laboratories, we used the AAV-DJP2 capsid variant to deliver CRISPR/Cas9 and guide RNAs (gRNAs) or shRNAs to THP-1 monocytic-like cells or to human monocyte-derived macrophages, respectively.[44,45] Finally, we reported the use of AAV1P4 and AAV1P5 for transduction of murine embryonic fibroblasts in the context of cellular reprogramming efforts,[46] and we have recently harnessed the same capsids as well as AAV9A2 and AAVrh.10A2 for robust CRISPR transfer in cultured human T cell lines (K.B., J.F., H.-G.K., and D.G, unpublished data). In all of these cases, we were pleased to see that data obtained in the initial screens with crude lysates were largely translatable to purified vectors; moreover, the reliability of our platform was independently confirmed in a direct side-by-side comparison of crude versus purified vectors in two cell lines (data not shown). These and more data from ongoing work showcase the power and potential of peptide display in non-AAV2 serotypes and create substantial optimism that others who are interested in *ex vivo* gene transfer will also greatly benefit from the new constructs and findings reported herein.

Importantly, while the present results were obtained in cultured cells, recent, as-of-yet unpublished data from the *in vivo* evaluation of our peptide-engineered capsid library highlight their superiority in primary mouse tissues and cells as well (J.W. and D.G., unpublished data). In this context, it is essential to note again that all of our *cap* gene variants were engineered to carry a frameshift that is corrected upon insertion of a peptide-encoding oligonucleotide. This is especially useful during large-scale generation of capsid libraries displaying randomized peptides, as it prevents contamination with capsids lacking a peptide. Based on our current data, we can readily anticipate that *in vivo* screening of such non-AAV2 peptide display libraries will complement existing AAV evolution technology and offer exclusive new opportunities to identify gene therapy vectors with desired features.

Irrespective of whether it is applied *ex vivo* or *in vivo*, a characteristic that our approach has in common with most of the already available technologies for AAV capsid diversification and stratification is that it acts "top-down," i.e., a wide collection of candidates is subjected to a screening or selection pressure in order to isolate the lead(s). As a result, and as opposed to "bottom-up" strategies that aim at rational capsid design, the biology underlying the properties of the final best performers typically remains obscure. While this may seem irrelevant as long as the vectors are functional and applied *ex vivo*, a deeper understanding of the biology of engineered AAV capsids becomes key once they are administered to human patients. Furthermore, insights into the functionality of ectopic peptides that are grafted onto AAV capsids, and into the secondary effects this may have on capsid conformation, will inform and streamline future efforts at rational capsid engineering.

Therefore, in the past, multiple groups, including our own, have already speculated on possible mechanisms that are triggered by peptide insertion into AAV, including improved or restored heparin/HSPG binding,[6,47] specific receptor recognition,[10] enhanced cellular uptake,[48] acceleration of post-entry mechanisms,[22] or mimicking of host proteins such as cadherins.[8] Intriguingly, one can find common notions in many reports, including the present one, that provide additional clues and rules for future rational optimization. Perhaps most remarkable is that peptides with an NXXRXXX motif not only boost the efficacy of AAV2 and thus were often enriched, but that they also improve several other serotypes, as seen here, e.g., with peptides P4, P5, A2 or A6. Notably, data from Perabo et al.[6] as well as Körbelin et al.[47] suggest that an asparagine in position 1 and the presence of positively charged residues (such as arginine) elsewhere within the peptide confer a heparin/HSPG-binding phenotype to the engineered AAV2 capsid. Strikingly, though, Naumer et al.[48] provided conflicting evidence that display of peptide NDVRSAN (P4 in the present study) on AAV2 actually decreases cell binding and instead enhances vector endocytosis.

At this point, our own finding that these peptides enhanced various serotypes beyond AAV2 in numerous cell types cannot conclusively resolve this conundrum, but it may suggest that they indeed improve a common intracellular capsid processing step, rather than mediating binding to a specific cell surface receptor that is shared among all targeted cells. In line with this, we observed a strong and expected inhibition of transduction with wild-type AAV2 and AAV3 in heparin competition assays, but marginal to no effects with any other natural or peptide-modified capsid (data not shown). Similarly, in parallel assays where we pre-treated HeLa cells with neuraminidase type III from *Vibrio cholerae* to remove sialic acid from the cell surface, we saw the expected inhibition of AAV1, AAV5, and AAV6 (which all use *O*-linked sialic acid as primary receptor), but no impact on any peptide-modified variant of any serotype (data not shown). The only and remarkable exception was AAV9 and its derivatives whose transduction efficiency was actually higher in the treated cells. This is readily explained by the fact that AAV9 binds N-terminal galactose, which is masked by sialic acid on the cell surface and hence becomes accessible upon neuraminidase treatment.[49] Thus, our data suggest that peptide insertion had not completely abolished primary receptor binding in AAV9 but still improved the efficiency of the capsid, most likely also by enhancing intracellular steps.

Generally, we surmise that peptides inserted into AAV most likely mediate pleiotropic effects whose extent is determined by subtle differences in numerous parameters, comprising the capsid scaffold, the position, number, and nature of residues flanking the insertion, and the target cell. This is well in line with our observations that even the mostly potent NXXRXXX motifs failed to enhance particular serotypes in specific cells, that we saw differences between individual NXXRXXX variants (e.g., Figure 6), and that the transduction efficiency of peptide-modified AAV2 varied drastically based on the flanking residues, insertion site, and NXXRXXX permutation (Figure 7). Thus, while we consider NXXRXXX motifs as overall beneficial and a good starting point for future vector or library designs, we also recognize a need to better dissect the functionality of these and other peptides *ex vivo* and *in vivo*. To this end, we think that the comprehensive list of constructs and associated transduction results reported in this study and accessible online provide useful starting points for additional investigations into the underlying biology and for the identification of possible common principles. Accelerating and facilitating this process should be the simplicity with which new peptide-modified AAV capsids can be generated based on our plasmid templates, in conjunction with the feasibility to transfer interesting capsid variants between laboratories in dried and pre-arrayed form, as exemplified in Figure 8. A rewarding future research topic should then be to quantify and compare vector copy numbers versus AAV mRNA or protein expression in cells transduced with different capsid variants, to unravel at which step the peptides are active, and to generally untangle the frequently observed discrepancies between AAV DNA, RNA, and protein levels in cells (also *in vivo*; J.W. and D.G., unpublished data). Finally, a particularly intriguing strategy to extract and harness specific features from the present and future peptide variants could be to apply machine learning, with the aim to further streamline capsid library design or to even achieve the ultimate goal in molecular AAV capsid evolution, i.e., rational engineering. Until then, by demonstrating the great potential of alternative AAV serotypes as platforms for peptide display, we hope that the data reported herein will encourage others to also start exploring this largely neglected but very potent approach at AAV vector optimization.

## MATERIALS AND METHODS

### Cloning Procedures

Cloning of all helper plasmids expressing AAV2 *rep* together with unmodified *cap* of different serotypes including AAV-DJ has been reported recently.[39,50,51] In these constructs, the *cap* open reading frames are flanked by a 5′ SwaI site and a 3′ SpeI site, permitting easy swapping by directional cloning. To introduce oligonucleotides encoding specific peptides into the different capsid genes, we first engineered two unique SfiI restriction sites into the corresponding AAV helper construct and then used a two-fragment cloning strategy (see Figure 1). Therefore, the first approximately 1.8 kb of every *cap* gene were PCR amplified using a suitable forward primer containing a SwaI site together with a reverse primer carrying SfiI and NsiI sites at its 3′ end. All primer sequences used in this work are available from the authors upon request. In a second, parallel PCR, the residual approximately 400 bp of each capsid gene were amplified with a forward primer that contained the same sites in a reverse order, i.e., NsiI at the 5′ end followed by SfiI, and with a reverse primer comprising a SpeI site. Both PCR fragments were digested with NsiI and either SwaI (5′ *cap* fragment) or SpeI (3′ *cap* fragment) and then ligated into the SwaI/SpeI double-digested helper plasmid backbone. This resulted in a full-length *cap* gene containing two new SfiI sites for later insertion of the peptide-encoding oligonucleotides. Correct sequence composition and the presence of the two SfiI sites were confirmed by sequencing. Of note, the SfiI-based insertion sites were designed such that they introduced a frameshift into the capsid genes (circled in Figures 1A and 1B). Only upon correct oligonucleotide insertion, the reading frame is shifted back to the original. Annealed peptide-encoding oligonucleotides contained two overhangs matching the SfiI sites and were ligated into the SfiI-digested backbone. Forward DNA sequences encoding the pre-selected peptides are shown in Table S2. To clone the NXXRXXX motifs studied in Figure 6, the forward sequence AAC $(NNB)_2$ CGC $(NNB)_3$ was inserted using our previously reported library cloning strategy,[24] where N is any nucleotide and B is C, G, or T but not A, to reduce the frequency of stop codons in the ensuing library. Correct insertion was confirmed by sequencing. The AAV2 variants with different peptide-flanking residues in Figure 7 were generated through overlap-extension PCR. In all cases, full oligonucleotide or primer sequences, respectively, are available from the authors upon request.

### Cell Culture

Cells were typically maintained and grown in Dulbecco's modified Eagle's medium (DMEM; Life Technologies, Carlsbad, CA, USA) supplemented with 10% fetal calf serum (FCS; Biochrom, Berlin, Germany), 100 U/mL penicillin, 100 μg/mL streptomycin, and 2 mM L-glutamine (all Life Technologies). Details on the culturing conditions for specific cell types used in this work are available from the authors upon request.

### Small-Scale AAV Vector Preparations

Small-scale AAV vector stocks ("crude lysates") were produced essentially as reported before,[50,51] using a standard triple transfection protocol in six-well plates. Briefly, $3.5 \times 10^5$ HEK293T cells were seeded per well in a volume of 4 mL of DMEM plus antibiotics, and transfected 24 h later using TurboFect transfection reagent and following the manufacturer's instructions for this format (Thermo Scientific, Waltham, MA, USA). The transfection mixture contained equal amounts (1.3 μg of each) of the three plasmids required for vector production, i.e., the AAV helper plasmid encoding *rep* of AAV2 and *cap* of the selected variant, an adenoviral helper plasmid, and the vector construct encoding the luciferase or YFP reporter. Around 72 h later, the medium was removed, and AAV particles were extracted from the cells as reported[50,51] with slight modifications (resuspension in 300 μL of 1× PBS, five freeze-thaw cycles, 10 min centrifugation at 16,100 × *g* to remove debris) and stored in aliquots at −80°C for later use.

### Transduction Assays

Transduction was usually carried out in a 96-well format, by adding 10 μL of per crude lysate with a multichannel pipette directly into the medium of the pre-plated cells. Alternatively, the crude lysates were added during cell plating. Forty-eight to 72 h later, YFP expression was measured by microscopy or FACS analysis (see below), or by luciferase assay (Promega, Mannheim, Germany).

### Microscopy-Based Assay in Well Plates

For microscopy analysis, cells were fixed with 4% paraformaldehyde for 30 min and subsequently stained with Hoechst. Images were acquired on an epifluorescence Scan^R screening microscope equipped with the Scan^R acquisition software (Olympus Biosystems, Münster, Germany) in the Hoechst and YFP channels. A 10× objective was used to measure 9–16 positions per well with appropriate excitation and emission filters. Subsequently, the images were processed via our previously established pipeline for quantitative image analysis.[52] Main readouts of the image analysis were the overall mean gray value over all cells in the image, the total cell count, and values for AAV transduction efficiencies, i.e., percentages of YFP-positive cells.

### Flow Cytometry Analysis of AAV Transduction

Transduction rates and mean fluorescence intensities of YFP-expressing AAV vectors were determined by flow cytometry. Cell size and granularity were determined by forward and sideward scatter. Cells were defined as "alive" according to these parameters, gated for measurement of YFP fluorescence in the yellow channel, and plotted against red fluorescence. Background fluorescence caused by autofluorescence of, e.g., dying cells was determined using untransduced samples, and the threshold for fluorescence-positive cells was set according to this value. Transduction rates were determined as percentage of positive cells out of at least 5,000 events in the alive cells gate. Mean fluorescence intensities reflecting the expression intensity per cell were calculated from the total of fluorescence-positive cells. For comparison of transduction rates and intensities between different cells, forward and sideward scatter as well as the definition of alive cells were adjusted to the properties (size and density) of the respective cell type. Detector intensities were kept constant for all measurements within one cell type to permit fair comparisons. All data were acquired with a Cytomics FC500MPL analyzer flow cytometer (Beckman Coulter, Brea, CA, USA) in a 96-well format.

### Spotting

For AAV coating on 96 well-plates, 5 μL of crude lysate was mixed with 0.39 μL of a freshly prepared 0.2% gelatin solution (Sigma-Aldrich, St. Louis, MO, USA) containing 1% fibronectin (Sigma-Aldrich), 0.35 μL of a freshly prepared 1% sucrose (USB, Cleveland, OH, USA) solution in Opti-MEM medium (Invitrogen, Carlsbad, CA, USA), and 19.27 μL of $H_2O$ to yield a total volume of 25 μL, which is sufficient to cover one well of a 96-well plate. For 384 well-plates, a total volume of 10 μL was used per well. Therefore, 2 μL of crude lysate was mixed with 0.15 μL of 0.2% gelatin solution containing 1% fibronectin, 0.14 μL of Opti-MEM medium with 1% sucrose, and 7.71 μL of $H_2O$. Plates were stored at −20°C overnight and dried the next day in a freeze dryer for 1.5 h. Dried plates can be stored at room temperature or at −20°C.

### Western Blot Analysis

To detect AAV Rep or VP proteins via western blotting, we followed our recently published semi-dry blotting protocol, using primary antibodies B1 (diluted 1:30 in blocking buffer) for detection of AAV capsid proteins VP1–VP3, or 303.9 (diluted 1:10) for detection of all four AAV Rep proteins (both antibodies were kind gifts from J. Kleinschmidt). As secondary antibody for subsequent detection by chemiluminescence, horseradish peroxidase-conjugated goat anti-mouse antibody (Jackson ImmunoResearch Laboratories, Cambridgeshire, UK) diluted 1:10,000 in blocking buffer was used. Bound antibodies were visualized with the Western Lightning Plus-ECL (enhanced chemiluminescence) reagent (PerkinElmer, Waltham, MA, USA) and by developing exposed X-ray films (GE Healthcare, Freiburg, Germany) in an X-Omat 2000 processor (Kodak, Rochester, NY, USA).

### Structural Modeling

Peptide sequences were incorporated into the VP3 sequence in different AAV serotypes at the positions listed in Table S1. The coordinates of the chimeric VP3-peptide models were generated from the resulting sequences, using each wild-type AAV PDB coordinate (RCSB PDB [https://www.rcsb.org/] and AAV7 [unpublished data]) as template in the SWISS-MODEL online tool (https://swissmodel.expasy.org/).[53] For AAVrh.10, AAVpo.1, and AAV12, the tool was allowed to select its own template since there are no available structures for these three viruses. The structural coordinates of peptide P2 (PDB: 1FUL) and K2 (PDB: 2FHL) were considered during model building by interactive rigid body rotations and translations into the AAV VP3 coordinates using the Coot program.[54] The AAV-peptide models were visualized in the Coot program for further comparisons of the VR-VIII insertion site between distinct AAV serotypes with the same peptide or different peptides displayed on the same AAV serotype. Cartoon representations of monomer and trimer as well as surface representations of 60-mers were generated using the PyMOL program.[36] The multimers (trimer and 60-mer) were generated by icosahedral matrix multiplication using the online application ViperDB (http://viperdb.scripps.edu/oligomer_multi.php)[55]. Depth-cue surface representations of wild-type AAV1 and AAV2 were generated using the UCSF-Chimera program.[37]

### Data Availability

The database SPIRIT is freely accessible online at http://spirit.cladiac.com/aav.html.

## SUPPLEMENTAL INFORMATION

Supplemental Information can be found online at https://doi.org/10.1016/j.ymthe.2020.02.009.

## AUTHOR CONTRIBUTIONS

K.B., E.K., J.W., A.S., J.F., L.Z., A.W., J.B., N.B., D.M., A.R., H.-G.K., H.E., M.M., and D.G. conceived and designed the experiments. K.B.,

E.K., J.W., A.S., J.F., L.Z., A.W., J.B., N.B., C. Schmelas, D.M., and A.R. performed experiments. C. Stüllein together with K.B. and P.B. generated the database SPIRIT. L.-Y.H. and M.A.-M. performed all AAV capsid modeling. E.W. was crucially involved in all AAV preparations. K.B. and D.G. wrote the manuscript with input from all other authors. All authors read and approved the final version.

## CONFLICTS OF INTEREST

K.B., J.W., A.S., M.M., and D.G. are inventors on multiple patent applications covering the use of different AAV variants for peptide display. D.G. is a co-founder and shareholder of AaviGen GmbH. C. Stüllein is a shareholder of CLADIAC GmbH. The remaining authors declare no competing interests.

## ACKNOWLEDGMENTS

K.B., H.-G.K., and D.G. are thankful for support by the German Center for Infection Research (DZIF, BMBF; TTU-HIV 04.803 and TTU-HIV 04.815). H.-G.K. and D.G. acknowledge funding by the German Research Foundation (DFG) through the Cluster of Excellence CellNetworks (EXC81) and the Collaborative Research Center SFB 1129 (project no. 240245660). C. Schmelas and D.G. appreciate additional support by the DFG via the Collaborative Research Center TRR 179 (project no. 272983813). D.G. is further grateful for funding through the MYOCURE project. MYOCURE has received funding from the European Union's Horizon 2020 research and innovation program under grant agreement no. 667751. J.F. and D.G. are thankful for funding from the Cystic Fibrosis Foundation (CFF, grant no. GRIMM15XX0) and the Heidelberg Biosciences International Graduate School (HBIGS) at Heidelberg University. J.B., N.B., E.W., and H.E. are also grateful for support from the Cluster of Excellence CellNetworks (DFG, EXC81). We thank Marina Bechtle for support during initial transduction analyses. We are moreover indebted to Anke-Mareil Heuser and David Bejarano (Department of Infectious Diseases/Virology, Heidelberg University Hospital, Heidelberg, Germany) for isolating, differentiating, and providing primary human monocyte-derived macrophages. In addition, we thank the following colleagues (in alphabetical order) for providing further cell types: Hilmar Bading, Anne-Kathrin Herrmann, Dirk Hose, Bettina Kempkes, Martina Muckenthaler, Walter Muranyi, Marlies Mürnseer, Anna De Oliveira, Marc Schneider, Anja Seckinger, Alica Torkov, and Ruth Brack-Werner. Moreover, we thank Walter Muranyi and Manuel Gunkel for help with microscopy. Finally, we are indebted to Carolin Schmelas from the Grimm laboratory for coining the acronym SPIRIT, and to Vera Sonntag-Buck (supported by DZIF and SFB 1129) for technical assistance in the revision phase.

## REFERENCES

1. Büning, H., and Srivastava, A. (2019). Capsid modifications for targeting and improving the efficacy of AAV vectors. Mol. Ther. Methods Clin. Dev. *12*, 248–265.
2. Grimm, D., and Zolotukhin, S. (2015). E pluribus unum: 50 years of research, millions of viruses, and one goal—tailored acceleration of AAV evolution. Mol. Ther. *23*, 1819–1831.
3. Govindasamy, L., Padron, E., McKenna, R., Muzyczka, N., Kaludov, N., Chiorini, J.A., and Agbandje-McKenna, M. (2006). Structurally mapping the diverse phenotype of adeno-associated virus serotype 4. J. Virol. *80*, 11556–11570.
4. Kotterman, M.A., and Schaffer, D.V. (2014). Engineering adeno-associated viruses for clinical gene therapy. Nat. Rev. Genet. *15*, 445–451.
5. Asokan, A., Schaffer, D.V., and Samulski, R.J. (2012). The AAV vector toolkit: poised at the clinical crossroads. Mol. Ther. *20*, 699–708.
6. Perabo, L., Goldnau, D., White, K., Endell, J., Boucas, J., Humme, S., Work, L.M., Janicki, H., Hallek, M., Baker, A.H., and Büning, H. (2006). Heparan sulfate proteoglycan binding properties of adeno-associated virus retargeting mutants and consequences for their in vivo tropism. J. Virol. *80*, 7265–7269.
7. Girod, A., Ried, M., Wobus, C., Lahm, H., Leike, K., Kleinschmidt, J., Deléage, G., and Hallek, M. (1999). Genetic capsid modifications allow efficient re-targeting of adeno-associated virus type 2. Nat. Med. *5*, 1052–1056.
8. Müller, O.J., Kaul, F., Weitzman, M.D., Pasqualini, R., Arap, W., Kleinschmidt, J.A., and Trepel, M. (2003). Random peptide libraries displayed on adeno-associated virus to select for targeted gene therapy vectors. Nat. Biotechnol. *21*, 1040–1046.
9. Perabo, L., Büning, H., Kofler, D.M., Ried, M.U., Girod, A., Wendtner, C.M., Enssle, J., and Hallek, M. (2003). In vitro selection of viral vectors with modified tropism: the adeno-associated virus display. Mol. Ther. *8*, 151–157.
10. Sallach, J., Di Pasquale, G., Larcher, F., Niehoff, N., Rübsam, M., Huber, A., Chiorini, J., Almarza, D., Eming, S.A., Ulus, H., et al. (2014). Tropism-modified AAV vectors overcome barriers to successful cutaneous therapy. Mol. Ther. *22*, 929–939.
11. Hordeaux, J., Yuan, Y., Clark, P.M., Wang, Q., Martino, R.A., Sims, J.J., Bell, P., Raymond, A., Stanford, W.L., and Wilson, J.M. (2019). The GPI-linked protein LY6A drives AAV-PHP.B transport across the blood-brain barrier. Mol. Ther. *27*, 912–921.
12. Matsuzaki, Y., Tanaka, M., Hakoda, S., Masuda, T., Miyata, R., Konno, A., and Hirai, H. (2019). Neurotropic properties of AAV-PHP.B are shared among diverse inbred strains of mice. Mol. Ther. *27*, 700–704.
13. Vandenberghe, L.H. (2019). AAV engineering identifies a species barrier that highlights a portal to the brain. Mol. Ther. *27*, 901–903.
14. Stachler, M.D., Chen, I., Ting, A.Y., and Bartlett, J.S. (2008). Site-specific modification of AAV vector particles with biophysical probes and targeting ligands using biotin ligase. Mol. Ther. *16*, 1467–1473.
15. Arnold, G.S., Sasser, A.K., Stachler, M.D., and Bartlett, J.S. (2006). Metabolic biotinylation provides a unique platform for the purification and targeting of multiple AAV vector serotypes. Mol. Ther. *14*, 97–106.
16. Sayroo, R., Nolasco, D., Yin, Z., Colon-Cortes, Y., Pandya, M., Ling, C., and Aslanidi, G. (2016). Development of novel AAV serotype 6 based vectors with selective tropism for human cancer cells. Gene Ther. *23*, 18–25.
17. Stachler, M.D., and Bartlett, J.S. (2006). Mosaic vectors comprised of modified AAV1 capsid proteins for efficient vector purification and targeting to vascular endothelial cells. Gene Ther. *13*, 926–931.
18. Koerber, J.T., Jang, J.H., Yu, J.H., Kane, R.S., and Schaffer, D.V. (2007). Engineering adeno-associated virus for one-step purification via immobilized metal affinity chromatography. Hum. Gene Ther. *18*, 367–378.
19. Michelfelder, S., Varadi, K., Raupp, C., Hunger, A., Körbelin, J., Pahrmann, C., Schrepfer, S., Müller, O.J., Kleinschmidt, J.A., and Trepel, M. (2011). Peptide ligands incorporated into the threefold spike capsid domain to re-direct gene transduction of AAV8 and AAV9 in vivo. PLoS ONE *6*, e23101.
20. Cronin, T., Vandenberghe, L.H., Hantz, P., Juttner, J., Reimann, A., Kacsó, A.E., Huckfeldt, R.M., Busskamp, V., Kohler, H., Lagali, P.S., et al. (2014). Efficient transduction and optogenetic stimulation of retinal bipolar cells by a synthetic adeno-associated virus capsid and promoter. EMBO Mol. Med. *6*, 1175–1190.
21. Raupp, C., Naumer, M., Müller, O.J., Gurda, B.L., Agbandje-McKenna, M., and Kleinschmidt, J.A. (2012). The threefold protrusions of adeno-associated virus type 8 are involved in cell surface targeting as well as postattachment processing. J. Virol. *86*, 9396–9408.
22. Varadi, K., Michelfelder, S., Korff, T., Hecker, M., Trepel, M., Katus, H.A., Kleinschmidt, J.A., and Müller, O.J. (2012). Novel random peptide libraries displayed on AAV serotype 9 for selection of endothelial cell-directed gene transfer vectors. Gene Ther. *19*, 800–809.
23. Deverman, B.E., Pravdo, P.L., Simpson, B.P., Kumar, S.R., Chan, K.Y., Banerjee, A., Wu, W.L., Yang, B., Huber, N., Pasca, S.P., and Gradinaru, V. (2016). Cre-dependent

selection yields AAV variants for widespread gene transfer to the adult brain. Nat. Biotechnol. *34*, 204–209.

24. Grimm, D., Lee, J.S., Wang, L., Desai, T., Akache, B., Storm, T.A., and Kay, M.A. (2008). In vitro and in vivo gene therapy vector evolution via multispecies interbreeding and retargeting of adeno-associated viruses. J. Virol. *82*, 5887–5911.

25. Tan, F., Chu, C., Qi, J., Li, W., You, D., Li, K., Chen, X., Zhao, W., Cheng, C., Liu, X., et al. (2019). AAV-ie enables safe and efficient gene transfer to inner ear cells. Nat. Commun. *10*, 3733.

26. Adachi, K., and Nakai, H. (2010). A new recombinant adeno-associated virus (AAV)-based random peptide display library system: infection-defective AAV1.9-3 as a novel detargeted platform for vector evolution. Gene Ther. Regul. *5*, 31–55.

27. Ying, Y., Müller, O.J., Goehringer, C., Leuchs, B., Trepel, M., Katus, H.A., and Kleinschmidt, J.A. (2010). Heart-targeted adeno-associated viral vectors selected by in vivo biopanning of a random viral display peptide library. Gene Ther. *17*, 980–990.

28. Khabou, H., Desrosiers, M., Winckler, C., Fouquet, S., Auregan, G., Bemelmans, A.P., Sahel, J.A., and Dalkara, D. (2016). Insight into the mechanisms of enhanced retinal transduction by the engineered AAV2 capsid variant -7m8. Biotechnol. Bioeng. *113*, 2712–2724.

29. Dalkara, D., Byrne, L.C., Klimczak, R.R., Visel, M., Yin, L., Merigan, W.H., Flannery, J.G., and Schaffer, D.V. (2013). In vivo-directed evolution of a new adeno-associated virus for therapeutic outer retinal gene delivery from the vitreous. Sci. Transl. Med. *5*, 189ra76.

30. Michelfelder, S., Kohlschütter, J., Skorupa, A., Pfennings, S., Müller, O., Kleinschmidt, J.A., and Trepel, M. (2009). Successful expansion but not complete restriction of tropism of adeno-associated virus by in vivo biopanning of random virus display peptide libraries. PLoS ONE *4*, e5122.

31. Shi, W., and Bartlett, J.S. (2003). RGD inclusion in VP3 provides adeno-associated virus type 2 (AAV2)-based vectors with a heparan sulfate-independent cell entry mechanism. Mol. Ther. *7*, 515–525.

32. Waterkamp, D.A., Müller, O.J., Ying, Y., Trepel, M., and Kleinschmidt, J.A. (2006). Isolation of targeted AAV2 vectors from novel virus display libraries. J. Gene Med. *8*, 1307–1319.

33. White, K., Büning, H., Kritz, A., Janicki, H., McVey, J., Perabo, L., Murphy, G., Odenthal, M., Work, L.M., Hallek, M., et al. (2008). Engineering adeno-associated virus 2 vectors for targeted gene delivery to atherosclerotic lesions. Gene Ther. *15*, 443–451.

34. Oi, J., Terashima, T., Kojima, H., Fujimiya, M., Maeda, K., Arai, R., Chan, L., Yasuda, H., Kashiwagi, A., and Kimura, H. (2008). Isolation of specific peptides that home to dorsal root ganglion neurons in mice. Neurosci. Lett. *434*, 266–272.

35. Terashima, T., Oka, K., Kritz, A.B., Kojima, H., Baker, A.H., and Chan, L. (2009). DRG-targeted helper-dependent adenoviruses mediate selective gene delivery for therapeutic rescue of sensory neuronopathies in mice. J. Clin. Invest. *119*, 2100–2112.

36. DeLano, W.L. (2002). The PyMOL molecular graphics system. Version 1.7.4 (Schrödinger, LLC).

37. Yang, Z., Lasker, K., Schneidman-Duhovny, D., Webb, B., Huang, C.C., Pettersen, E.F., Goddard, T.D., Meng, E.C., Sali, A., and Ferrin, T.E. (2012). UCSF Chimera, MODELLER, and IMP: an integrated modeling system. J. Struct. Biol. *179*, 269–278.

38. Kunze, C., Börner, K., Kienle, E., Orschmann, T., Rusha, E., Schneider, M., Radivojkov-Blagojevic, M., Drukker, M., Desbordes, S., Grimm, D., and Brack-Werner, R. (2018). Synthetic AAV/CRISPR vectors for blocking HIV-1 expression in persistently infected astrocytes. Glia *66*, 413–427.

39. Herrmann, A.K., Bender, C., Kienle, E., Grosse, S., El Andari, J., Botta, J., Schürmann, N., Wiedtke, E., Niopek, D., and Grimm, D. (2019). A robust and all-inclusive pipeline for shuffling of adeno-associated viruses. ACS Synth. Biol. *8*, 194–206.

40. Zinn, E., Pacouret, S., Khaychuk, V., Turunen, H.T., Carvalho, L.S., Andres-Mateos, E., Shah, S., Shelke, R., Maurer, A.C., Plovie, E., et al. (2015). In silico reconstruction of the viral evolutionary lineage yields a potent gene therapy vector. Cell Rep. *12*, 1056–1068.

41. Weinmann, J., and Grimm, D. (2017). Next-generation AAV vectors for clinical use: an ever-accelerating race. Virus Genes *53*, 707–713.

42. Lau, C.H., Ho, J.W., Lo, P.K., and Tin, C. (2019). Targeted transgene activation in the brain tissue by systemic delivery of engineered AAV1 expressing CRISPRa. Mol. Ther. Nucleic Acids *16*, 637–649.

43. Cordas Dos Santos, D.M., Eilers, J., Sosa Vizcaino, A., Orlova, E., Zimmermann, M., Stanulla, M., Schrappe, M., Börner, K., Grimm, D., Muckenthaler, M.U., et al. (2018). *MAP3K7* is recurrently deleted in pediatric T-lymphoblastic leukemia and affects cell proliferation independently of NF-κB. BMC Cancer *18*, 663.

44. Fanucchi, S., Fok, E.T., Dalla, E., Shibayama, Y., Börner, K., Chang, E.Y., Stoychev, S., Imakaev, M., Grimm, D., Wang, K.C., et al. (2019). Immune genes are primed for robust transcription by proximal long noncoding RNAs located in nuclear compartments. Nat. Genet. *51*, 138–150.

45. Bejarano, D.A., Peng, K., Laketa, V., Börner, K., Jost, K.L., Lucic, B., Glass, B., Lusic, M., Müller, B., and Kräusslich, H.G. (2019). HIV-1 nuclear import in macrophages is regulated by CPSF6-capsid interactions at the nuclear pore complex. eLife *8*, e41800.

46. Senís, E., Mosteiro, L., Wilkening, S., Wiedtke, E., Nowrouzi, A., Afzal, S., Fronza, R., Landerer, H., Abad, M., Niopek, D., et al. (2018). AAVvector-mediated in vivo reprogramming into pluripotency. Nat. Commun. *9*, 2651.

47. Körbelin, J., Hunger, A., Alawi, M., Sieber, T., Binder, M., and Trepel, M. (2017). Optimization of design and production strategies for novel adeno-associated viral display peptide libraries. Gene Ther. *24*, 470–481.

48. Naumer, M., Popa-Wagner, R., and Kleinschmidt, J.A. (2012). Impact of capsid modifications by selected peptide ligands on recombinant adeno-associated virus serotype 2-mediated gene transduction. J. Gen. Virol. *93*, 2131–2141.

49. Shen, S., Bryant, K.D., Brown, S.M., Randell, S.H., and Asokan, A. (2011). Terminal N-linked galactose is the primary receptor for adeno-associated virus 9. J. Biol. Chem. *286*, 13532–13540.

50. Grosse, S., Penaud-Budloo, M., Herrmann, A.K., Börner, K., Fakhiri, J., Laketa, V., Krämer, C., Wiedtke, E., Gunkel, M., Ménard, L., et al. (2017). Relevance of assembly-activating protein for adeno-associated virus vector production and capsid protein stability in mammalian and insect cells. J. Virol. *91*, e01198-17.

51. Herrmann, A.K., Große, S., Börner, K., Krämer, C., Wiedtke, E., Gunkel, M., and Grimm, D. (2019). Impact of the assembly-activating protein on molecular evolution of synthetic adeno-associated virus capsids. Hum. Gene Ther. *30*, 21–35.

52. Börner, K., Hermle, J., Sommer, C., Brown, N.P., Knapp, B., Glass, B., Kunkel, J., Torralba, G., Reymann, J., Beil, N., et al. (2010). From experimental setup to bioinformatics: an RNAi screening platform to identify host factors involved in HIV-1 replication. Biotechnol. J. *5*, 39–49.

53. Biasini, M., Bienert, S., Waterhouse, A., Arnold, K., Studer, G., Schmidt, T., Kiefer, F., Gallo Cassarino, T., Bertoni, M., Bordoli, L., and Schwede, T. (2014). SWISS-MODEL: modelling protein tertiary and quaternary structure using evolutionary information. Nucleic Acids Res. *42*, W252–W258.

54. Emsley, P., Lohkamp, B., Scott, W.G., and Cowtan, K. (2010). Features and development of Coot. Acta Crystallogr. D Biol. Crystallogr. *66*, 486–501.

55. Carrillo-Tripp, M., Shepherd, C.M., Borelli, I.A., Venkataraman, S., Lander, G., Natarajan, P., Johnson, J.E., Brooks, C.L., 3rd, and Reddy, V.S. (2009). VIPERdb$^2$: an enhanced and web API enabled relational database for structural virology. Nucleic Acids Res. *37*, D436–D442.